Microwave-Assisted Synthesis of Room Temperature Long Persistent Luminescent Materials and Their Imaging Applications

Yong Shen [1], Yunfei Xia [1], Ping Li [1], Shuo Zhang [1], Linlin Li [1], Die Hu [1], Dongfang Shi [2,*] and Kai Song [1,2,*]

[1] School of Life Science, Changchun Normal University, Changchun 130032, China; heiqpy1@tom.com (Y.S.); xiayunfei1103@163.com (Y.X.); chunlps@163.com (P.L.); zhangshuo727720@163.com (S.Z.); lin1805626597@163.com (L.L.); hudie18784775519@163.com (D.H.)

[2] Institute of Science, Technology and Innovation, Changchun Normal University, Changchun 130032, China

* Correspondence: shidongfang@ccsfu.edu.cn (D.S.); songkai@ccsfu.edu.cn (K.S.)

Abstract: In this study, we utilized a simple and efficient microwave heating method with polyethyleneimine (PEI) and phosphate as raw materials to synthesize room temperature persistent luminescence (RTPL) materials that emit phosphorescent light for up to 10 s. Our investigation revealed that the optimal synthesis conditions were a microwave radiation power of 560 W and a heating time of 5 min. The synthesized RTPL materials had an average particle size of 2 nm and exhibited excellent RTPL performance, with optimal excitation and emission wavelengths of 360 nm and 544 nm, respectively. Additionally, these materials displayed good water solubility. We conducted mapping experiments and in situ phosphorescent imaging of plants to showcase the potential applications of RTPL materials in the fields of biological imaging and anti-counterfeiting. Overall, our findings demonstrate the promising potential of these RTPL materials as versatile tools for various practical applications.

Keywords: long afterglow luminescent material; room temperature phosphorescence; microwave method; anti-counterfeiting; bioimaging

1. Introduction

Long afterglow luminescent materials are a type of photoluminescent material that can store energy from sunlight or ultraviolet light and emit light for minutes to hours after the excitation light is removed [1–4]. Due to this unique optical property, long afterglow luminescent materials find numerous applications in fields such as bioimaging, sensing, composition detection, optoelectronic devices, photocatalysts, optical information storage, information encryption, and anti-counterfeiting [5–13]. Conventional long afterglow luminescent materials include organometallic complexes and pure organic compounds without metals, with organometallic complexes being the standard choice. However, these materials have disadvantages, such as their high cost, cytotoxicity, poor stability, complicated preparation and purification processes, and the strict conditions required for producing an afterglow [14–17]. Pure organic long afterglow luminescent materials, however, are low cost and have a flexible molecular design [18], making them a viable alternative [19].

In recent years, researchers have made many efforts to prepare room temperature phosphorescent materials as better alternatives. Combinations of polymers and organic molecules have been used to achieve room temperature long afterglow luminescence or efficient long afterglow luminescence through the synergistic interaction of organic small molecules and polymers [20,21]. Furthermore, novel materials such as metal–organic framework materials (MOFs), conjugated polymers, carbon dots, and nanomaterials have been widely used in the preparation of room temperature phosphorescent materials [22–25]. These materials offer excellent long afterglow luminescence, simple preparation methods,

low production costs, good biocompatibility, and can be used in biomedical imaging, biomarkers, and pathology detection [5,26]. Recent research has also focused on embedding organic long afterglow materials into porous silicon dioxide (SiO_2) nanoparticles to prepare a new organic–inorganic composite material that can be applied in bioimaging [27].

The application and development of long afterglow luminescent materials have been impeded by the spin forbidden transition from the trilinear exciton to the ground state. To produce long afterglow luminescent materials with exceptional room temperature phosphorescence properties, two crucial factors must be addressed. Firstly, effective spin–orbit coupling can be achieved by promoting the inter-system crossing (ISC) process in order to efficiently populate the triplet state exciton. This can be accomplished by introducing transition metals, halogens, and aromatic carbonyl groups [16,28,29]. Secondly, the restriction of the transition from the lowest triplet state, the excited state (T1), to the ground state (S0) by non-radiative leaps can be achieved by crystallizing or embedding the luminescent material in a suitable substrate. This forms hydrogen bonds that limit the vibration and rotation of the luminescent group [19,30,31].

In this study, we have synthesized room temperature long afterglow luminescent materials in a single step using PEI and phosphoric acid with microwave-assisted heating. The use of PEI and phosphoric acid as nitrogen and phosphorus sources, respectively, is favorable for the $n{\rightarrow}\pi^*$ leap in the system, facilitating the filling of the triplet state inter-system crossover (ISC). Synthesis methods of organic room temperature phosphorescent materials mainly include the hydrothermal method, the template method, the pyrolysis method, and the microwave-assisted heating method. Water/solvothermal methods are when the solvents used in the system can affect the photoluminescence performance of the material [32]. The disadvantage of the template method is that the strong acids/bases used during the template removal process can affect the luminescent performance of RTPL materials [33]. The surface of RTPL materials synthesized via the pyrolysis method contains fewer functional groups, resulting in a decrease in luminescent performance [34]. The microwave-assisted heating method has significant advantages in this process compared with other synthetic methods. Microwave heating permits efficient heating and mixing in a brief amount of time, thereby expediting the synthesis of nanomaterials. It is a non-thermal equilibrium process with localized heating and selective heating that can synthesize nanomaterials of varying sizes, morphologies, and physicochemical properties under varying reaction conditions. In addition, microwave heating can uniformly heat the sample, thereby improving the uniformity and consistency of the synthesized nanomaterials. In terms of cost-effectiveness, microwave synthesis is an energy saving technique that can considerably reduce the reaction time and temperature as well as the energy consumption of chemical reactions and process pollution [35]. As a result, the microwave synthesis method has gained significant interest in the field of room temperature phosphorescent material preparation and has been widely used in recent years.

2. Materials and Methods

2.1. Materials and Instruments

Analytical grade solvents and compounds were used for preparation. The solvents and water used in our present work were redistilled and bubbled using N_2 for 1 min to eliminate O_2 without being specific. Phosphoric acid and polyethylenimine (PEI, mw = 1800–3000) were purchased from Alfa Aesar. All photoluminescence spectra were measured on a Hitachi F-4500 fluorescence spectrophotometer equipped with a continuous 150 W Xe arc lamp and a 10 mm quartz cuvette. The excitation and emission wavelength bandpasses were both set at 5 nm. Absorption spectra were recorded with a Shimadzu UV-3000 spectrophotometer. The microwave oven used was a Granz P70F23P-G5 (SO). The morphological and structural characteristics of the samples were analyzed via transmission electron microscopy (TEM) (JEOL). The organic functional groups and elemental composition of the sample surfaces were detected via Fourier transform infrared spectroscopy (FTIR) (PerkinElmer) and X-ray photoelectron spectroscopy (XPS) (Thermo Fisher Scientific). Ther-

mal gravimetric curves were measured using a TGA/DSC1 thermal analyzer from Mettler Toledo. The dispersion stability and particle size distribution of the samples in aqueous solution were analyzed using zeta potential and dynamic light scattering (DLS) (Malvern Panalytical). Finally, the optical properties of the samples were characterized, mainly to study the afterglow properties of the prepared materials.

2.2. Synthetic Procedures of RTPL Materials

Using a 100 mL beaker, 16 mL of ultrapure water and 2 mL of polyethylene imine were adding sequentially, and then phosphoric acid was added drop-wise into the solution. After stirring evenly, it was place in a preheated microwave oven to control the radiation power and time. The synthesized RTPL material was allowed to settle, and the resulting mixture solidified into a dark brown gel-like substance that was dissolved overnight by adding 40 mL of ultrapure water. The aqueous solution of the crude product was centrifuged (10,000 rpm/min for 20 min) and the supernatant was again filtered through a 0.22 m disposable filter to remove small impurities. The obtained filtrate was dialyzed in ultrapure water using a 1000 Da dialysis bag for three days (72 h), during which the water was changed seven times. The dialyzed samples were then freeze-dried to produce desiccated powder samples. They were locked up and stored. By controlling the radiation conditions and preparing samples at three different radiation powers and times (490 W, 6 min; 560 W, 5 min; and 630 W, 4 min), the optimal conditions for synthesizing RTPL materials were obtained. When the radiation power was 560 W and the radiation time was 5 min, the prepared sample had the best luminescence performance.

3. Results and Discussion

3.1. Design and Synthesis of RTPL Materials

In this study, we utilized a one-step microwave synthesis approach to prepare a long afterglow luminescent material. PEI and phosphoric acid were chosen as the experimental raw materials (as shown in Scheme 1a). Upon completion of the synthesis, we observed that the reactants had transformed into a dark brown, gel-like substance with a pungent burning odor. The resulting sample was allowed to cool to room temperature and subsequently subjected to centrifugation, filtration, dialysis, and vacuum freeze-drying to obtain a light brown solid product (Scheme 1b). In order to explore the best mode of synthesizing organic room temperature phosphorescent materials, we adopted the same synthesis conditions as before and selected amino compounds (N,N-dimethylaniline, azodiisobutyronitrile, ammonium dihydrogen phosphate, and N,N-dimethylformamide) similar to phosphoric acid and PEI to synthesize the RTPL materials. The RTPL materials synthesized by the four amine containing compounds mentioned above are listed as group A, group B, group C, and group D. No significant RTP was observed in groups A and B, and weak phosphorescence was observed in groups C and D, but the phosphorescence intensity was lower than that of the RTPL materials synthesized by PEI and phosphoric acid.

3.2. Characterization of the RTPL Materials

The long afterglow luminescent material which was prepared in this study exhibits good dispersion and a spherical or nearly spherical morphology with an average particle diameter of 2 nm (Figure 1a). The small particle size of the material significantly enhances its surface area and reactivity, making it a promising candidate for various applications, such as fluorescent probes, biosensing, and chemical analysis. The TEM images of the samples confirm the morphological and structural features of previously reported long afterglow luminescent materials [36,37], thereby demonstrating that similar materials to carbon dots can be synthesized through the microwave heating of PEI and phosphoric acid [16,30].
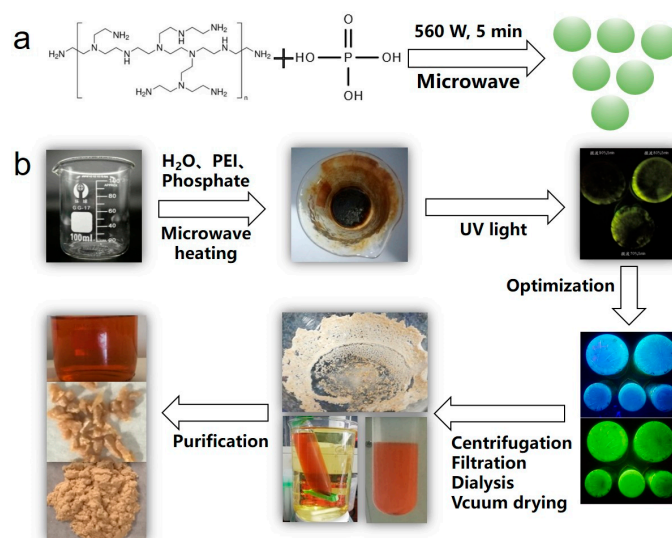
Scheme 1. Synthetic paths of RTPL materials. Schematic illustration of procedures for the preparation of RTPL materials (**a**) and the preparation process of RTPL materials (16 mL ultrapure water, 2 mL PEI mixed with phosphoric acid, 560 W microwave irradiation for 5 min, centrifugation, filtration, dialysis, and vacuum freeze drying can be used to obtain solid RTPL materials) (**b**).
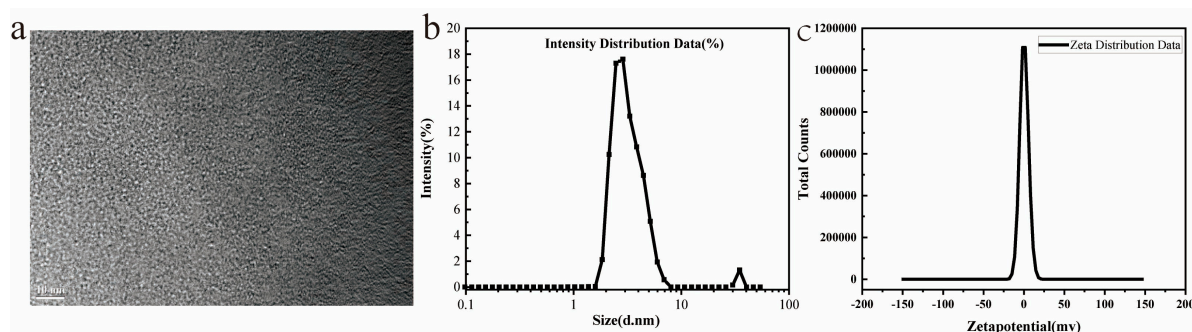

Figure 1. TEM (**a**), DLS (**b**), and zeta potential (**c**) of RTPL materials.

As depicted in Figure 1b, the particle size distribution of the sample solution was determined using two distinct techniques: DLS and TEM. The measured particle size distribution via DLS appeared relatively larger than that via TEM, which can be attributed to the amount of solvent in the sample in the DLS measurements. Notably, the hydrated particle diameters measured via DLS indicated the presence of surface groups in the sample solution, which likely contributed to its good water solubility [38].

The stability of a colloidal particle system is closely related to the magnitude of its zeta potential. A highly positive or negative zeta value can induce a significant repulsive force that impedes the aggregation of colloidal particles. Typically, a minimum zeta value of ±30 mV is required to ensure the stability of a colloidal particle system [39]. Nonetheless, the stability of the colloidal particle system is influenced by both electrostatic repulsive forces and van der Waals gravitational forces. The zeta potential only reflects the magnitude of the electrostatic repulsive force and cannot indicate the strength of the van der Waals gravitational forces. Therefore, a low absolute value of zeta potential does not necessarily imply an unstable colloidal particle system [40].

In the case of the microwave-assisted synthesis of long afterglow luminescent materials, Figure 1c reveals an absolute value of zeta potential within 20.00 mV. This measured value may be attributed to the limited number of functional groups, such as amino or carboxyl groups, that can undergo protonation in the sample solution. Despite the relatively low zeta potential, the colloidal particle system remains stable.

In this study, the surface organic functional groups of the prepared long afterglow luminescent materials were characterized via FTIR analysis, as depicted in Figure 2a. The stretching vibration zone above 3000 cm^{-1} is unsaturated C–H, which may be olefins or alkynes. Between 3200 and 3650 cm^{-1} is the stretching vibration of the hydroxyl OH or the hydrogen bonds, and between 3500 and 3100 cm^{-1} is the absorption of the N–H stretching vibration. Between 2100 and 2400 cm^{-1}, there are triple bonds and accumulated double-bond regions. The stretching vibration zone of the carboxyl group C=O is located between 1630 and 1680 cm^{-1}. C–H out-of-plane vibration bending occurs at 670–880 cm^{-1}.
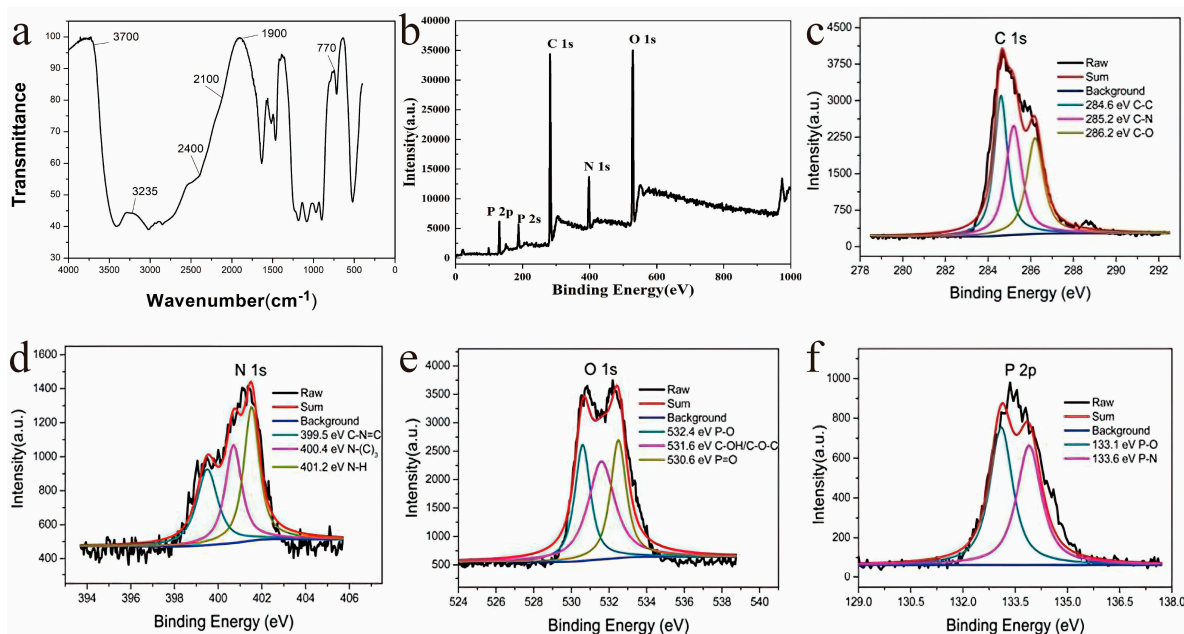

Figure 2. FTIR spectra (**a**), XPS full spectra (**b**), C 1s spectra (**c**), N 1s spectra (**d**), O 1s spectra (**e**), and P 2p spectra (**f**) of RTPL materials.

To confirm the FTIR results and further determine the chemical composition or elemental composition of the samples, X-ray photoelectron spectroscopy (XPS) analyses were conducted. The full scan XPS spectrum of the sample presented in Figure 2b showed characteristic peaks of P2p, C1s, N1s, and O1s at 131.17 eV, 283.36 eV, 395.79 eV, and 529.71 eV, respectively. The fractions of C, N, O, and P in the sample were determined to be 57.6%, 12.58%, 22.94%, and 6.88%, respectively. The C1s spectra indicated the presence of C–C/C=C (284.6 eV), C–N (285.2 eV), and C–O (286.2 eV) bonds in the long afterglow powder (Figure 2c). The N1s spectra showed three peaks at 399.5, 400.4, and 401.2 eV, corresponding to C–N=C, N–(C)3, and N–H bonds, respectively (Figure 2d). The O1s spectra had three peaks at 530.6, 531.6, and 532.4 eV, corresponding to P=O, C–OH/C–O–C, and P-O bonds, respectively (Figure 2e). The P2p spectra exhibited two peaks at 133.1 and 133.6 eV, corresponding to P-O and P-N bonds, respectively (Figure 2f). These XPS results, combined with the FTIR analysis, confirmed the presence of organic functional groups such as –OH, C–H, N–H, C–O, C=O, C–C=N, P=O, and C-N on the surface of the prepared long afterglow luminescent materials. These organic functional groups contribute to the good water solubility of the material.

3.3. Optical Properties of RTPL Materials

The long afterglow luminous material exhibits different properties in its solution and solid states. In natural light, the material appears brown in solution and light yellow in its solid form. When exposed to UV lamp radiation, the dissolved material does not emit light, while the solid state material exhibits blue fluorescence. When the UV lamp is turned off, the solid state material emits green phosphorescence. Figure 3a displays the phosphorescence

emission spectrum of the prepared long afterglow luminescent material. When excited with UV light at 360 nm, the material emits phosphorescence, with the highest intensity at 544 nm. This indicates that the material possesses excitation-dependent phosphorescence properties. Moreover, under observation with the naked eye, the solid-state long afterglow luminescent material shows a clear and distinct green phosphorescence that lasts for approximately 10 s after UV light irradiation has stopped, as shown in Figure 3b.
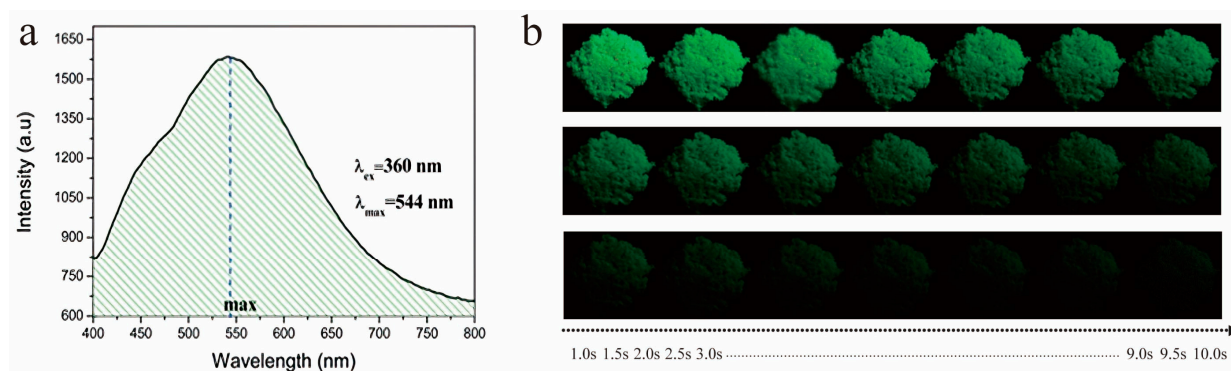

Figure 3. Phosphorescent spectra (**a**) and photos of light intensity over time (**b**) of RTPL materials.

As can be seen from Figure 4a, the phosphorescence intensity of the prepared long afterglow luminescent materials exhibits a distinct three-exponential decay. It is commonly accepted that this three-exponential decay is caused by complex jumps between multiple energy levels, including the self-excitation and self-compounding of electrons. The shape of the fluorescence decay curve is determined by energy transfer and electron leaping in the material. In the case of long afterglow luminescent materials, the excited electrons can remain in an excited state for an extended period after the excitation has ended before releasing energy in a triple-exponential form [41]. Therefore, the prepared long afterglow luminescent materials exhibit typical phosphorescence characteristics.
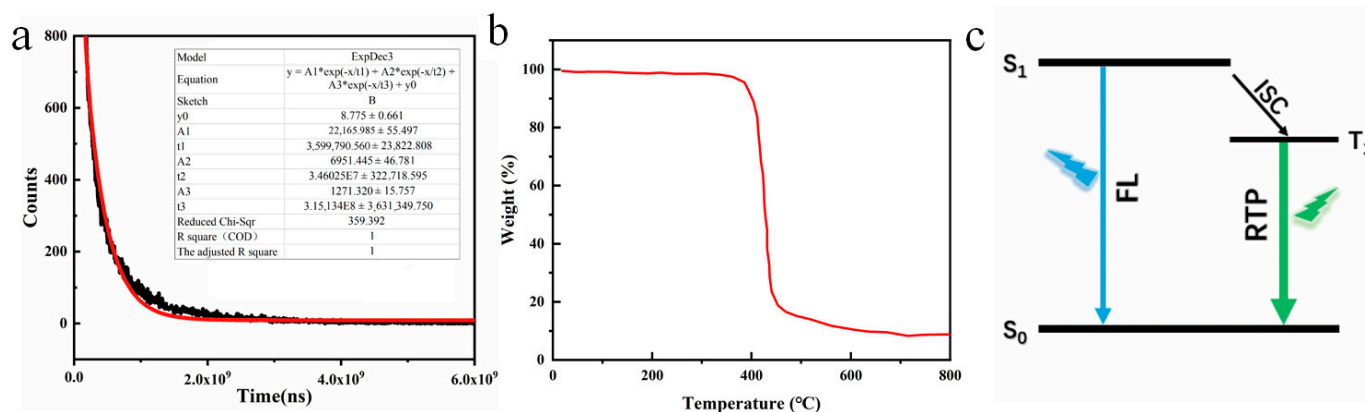

Figure 4. Phosphorescence decay curves for long afterglow materials (**a**), thermo-gravimetric analysis (TGA) curves (**b**), and a schematic of the room temperature phosphorescence (RTP) emission mechanism (the absorption process is omitted and the width of the emission line is used to roughly represent the intensity of fluorescence or room temperature phosphorescence emission) (**c**).

The mechanism underlying the fluorescence and phosphorescence emission from solid-state long afterglow materials is as follows. Initially, a PEI and phosphoric acid solution undergoes dehydration, condensation, cross-linking polymerization, and carbonization through microwave heating at approximately 200 °C. The microwave heating process leads to the formation of a highly cross-linked chemical structure in the material, which suppresses the nonradiative transition of triplet excitons. This phenomenon is known as the crosslink-enhanced emission (CEE) effect [42]. The FTIR and XPS characterization

results demonstrate that the prepared long afterglow luminescent materials are abundant in organic functional groups such as –OH, C–H, N–H, C–O, C=O, C–C=N, P=O, and C-N. Some of these organic functional groups, such as C=O and C–C=N, are responsible for the luminescence. The large number of organic functional groups formed on the surface of RTPL materials indicate that the carbonization process is incomplete [43]. This can also be demonstrated in the TGA curves of RTPL materials (Figure 4b). In addition to FTIR and XPS, which are used to analyze the types and structures of chemical bonds formed by phosphoric acid and polyacetamide as raw materials in RTPL, the thermal stability of both materials also affects the thermal decomposition process of long afterglow luminescent materials, thus affecting the characteristics of thermogravimetric curves. The luminescent properties of nanomaterials are affected by many factors, such as the chemical composition, crystal structure, surface modification, etc. [41]. TGA curves can provide information related to these factors, such as the decomposition characteristics of materials at high temperatures, the decomposition of surface functional groups, and so on, which can influence the luminescent properties of materials [44]. The thermogravimetric process of RTPL materials can be divided into four stages. The first stage is between 25 and 100 °C, which is mainly water evaporation. The second is between 400 and 460 °C, the main stage of weight loss. The rate of weight loss is about 75%, which is mainly caused by the decomposition of RTPL materials. The rate of weight loss is about 10% at the slow weight loss stage between 460 and 600 °C, which is related to the continuous pyrolysis of the remaining organic materials. The end stage of thermal decomposition is between 600 and 800 °C. Additionally, phosphoric acid and PEI can form hydrogen bonds, which can inhibit the nonradiative leap of trilinear excitons [14]. Lastly, PEI and phosphoric acid can provide N and P elements, respectively, and N and P element doping has been shown to favor the n→π* leap, thus facilitating the effective filling of the tristate exciton by ISC (Figure 4c), ultimately leading to the room temperature phosphorescence phenomenon [14,28,45]. The reason why long afterglow luminescent materials fail to emit phosphorescence in aqueous solutions is that the trilinear excitons of organic compounds are susceptible to nonradiative leaps due to the vibration and rotation of covalent bonds. Furthermore, phosphorescence can be easily quenched by the aqueous environment and dissolved oxygen [29,46].

3.4. Information Encryption and Anti-Counterfeiting

The prepared long afterglow luminescent material exhibits room temperature phosphorescent properties, making it suitable for various applications such as information encryption and anti-counterfeiting. In particular, it can be used as a special anti-counterfeiting ink, as illustrated in Figure 5. A solution of RTPL materials with a concentration of 1 mg/mL was prepared and evenly sprayed onto a hollow template with a pattern on the surface using a small spray bottle. After the template was dried, colored patterns were obtained (Figure 5a). When exposed to a 360 nm UV lamp, the ink emits blue fluorescence similar to conventional fluorescent ink (Figure 5b). However, upon turning off the UV lamp, the pattern emits green phosphorescence for several seconds (Figure 5c), which can be easily distinguished by the naked eye.

Figure 5d–f demonstrates the use of long afterglow luminescent material ink as a special encryption ink. Brown dye and RTPL materials were used to write on A_4 printing paper with a calligraphy pen. After drying, photographs were taken under natural light and a 360 nm UV light, respectively. When using fluorescent ink with a similar color on ordinary A_4 paper to write "UN" and long afterglow luminescent material ink to write "HAPPY", observation with the naked eye of the two colors is almost the same. However, when irradiated with an ultraviolet lamp, the blue fluorescent "UNHAPPY" can be observed, and only when the ultraviolet lamp is turned off can the green phosphorescent-encrypted information "HAPPY" be seen. This achieves the role of information encryption and decryption, indicating that the produced long afterglow ink can be used as a special encryption ink.

Figure 5. Photographs of patterns and words drawn on A$_4$ paper with a long afterglow material solution. Patterns under daylight (**a**) with text (**d**), patterns under UV light (**b**) with text (**e**), and patterns under darkness (**c**) with text (**f**).

Furthermore, the long afterglow ink exhibits particularly stable properties in the natural environment, as it is not affected by air humidity or temperature. The phosphorescent light emitted by the prepared long afterglow material after UV excitation remains bright for up to 30 days.

3.5. In Situ Long Afterglow Imaging of Celery

Although fluorescence imaging technology is widely used in biological imaging [47,48], biological samples exhibit endogenous fluorescence (background interference) that may overlap with the emission wavelength of the target fluorescence. Phosphorescence imaging is performed after removing the excitation light, does not require real-time imaging, and has a higher signal-to-noise ratio, which can suppress background fluorescence interference [5,22,30]. As shown by the optical data above, the prepared long afterglow luminescent materials have excellent phosphorescent properties, which can be applied to biological imaging experiments. Healthy celery stems were selected and cultivated in a solution of 1 mg/mL of RTPL materials. The growth status of the celery was observed and recorded every 24 h. After 3 days, a young and tender section was sliced by hand and pressed, dried, and observed under a fluorescence microscope. After 24, 48, and 72 h, in the vascular bundles of celery stems, a large amount of long afterglow materials is distributed, indicating that nanoscale RTPL materials can function within celery (Figure 6a). This is supported by the fact that the previous TEM confirmed the small particle size of RTPL materials. Since the RTPL material solution is more viscous than the plant culture solution, their migration behavior within the celery stem should be attributed more to active uptake than to passive syphoning. We also discovered that the treated celery plants remained fresh and upright, indicating that the solutions of the RTPL materials had low phytotoxicity and did not affect the celery's biological behavior in terms of continued survival and water uptake over the course of the three-day experimental period. This may be because the surface of the long afterglow luminescent material is rich in functional groups such as C=N, C=O, –OH, N–H, and –CH, which can interact specifically with biomolecules. These interactions can promote the dispersion and degradation of particles in the organism, thereby reducing the toxicity and side effects of particles and increasing the stability of particles in the organism. Among

them, bonds such as C=O, –OH, and N–H can interact with biomolecules through hydrogen bonds or van der Waals forces, thereby improving the biocompatibility and biodegradability of particles [49]. Functional groups such as hydroxyl and amino groups on the material surface can improve the degradation and metabolism of polymer nanoparticles in the body and reduce their damage to biological tissues [50]. As seen in the longitudinal section of the celery stem (Figure 6b), the field of view contains numerous brown particulate materials, indicating that the long afterglow luminescent material in the celery stem is not always monodisperse. When the particle size of the material is below a certain threshold, it tends to aggregate due to excessive surface tension, and the surrounding biological environment may also be a factor in particle aggregation. After UV excitation, fluorescence micrographs of celery stems were observed, and the images clearly revealed the internal structure of celery stems due to the absence of background light and autofluorescence; the green tubular image represents the vascular structure of celery stems (Figure 6b).
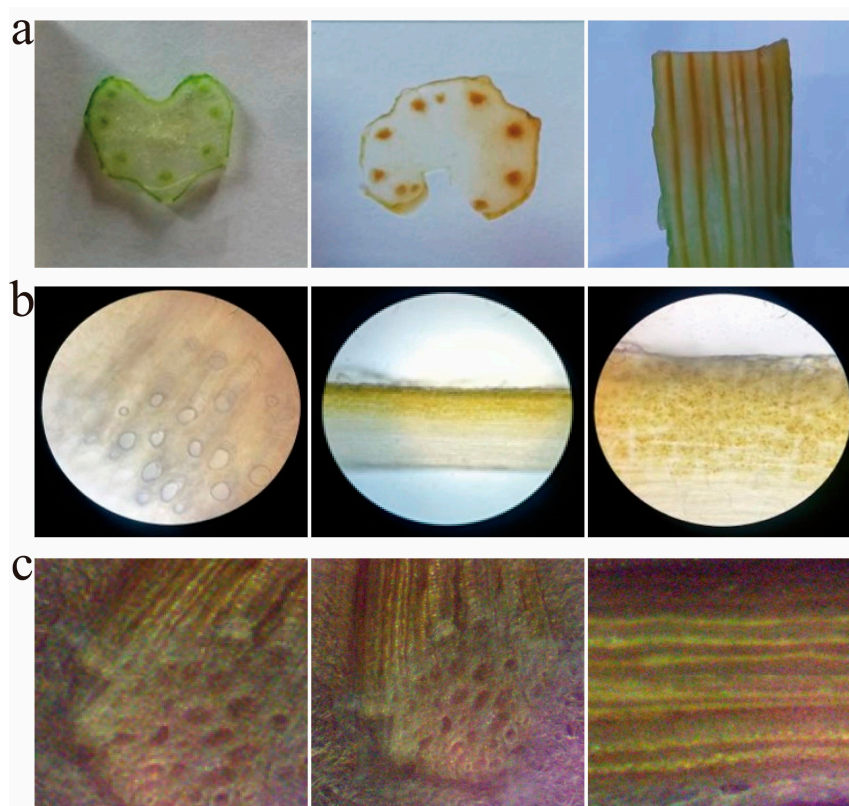

Figure 6. Stems of celery soaked in a long afterglow material solution. Photographs of transverse and longitudinal sections (**a**), microscopic images in daylight (**b**), and microscopic images of vascular bundles after immediate cessation of excitation by UV light (**c**).

4. Conclusions

Long afterglow luminescent materials that can emit blue fluorescence under UV irradiation and room temperature phosphorescence for 10 s after stopping UV excitation were synthesized via the microwave-assisted heating method. By characterizing the optical properties, morphological structure, and organic functional groups on the surface of the samples, the reasons why the long afterglow luminescent materials synthesized with PEI and phosphoric acid exhibit room temperature phosphorescence under ambient conditions were analyzed, concluding that this was due to the formation of hydrogen bonds and the doping of N and P elements. The formation of hydrogen bonds can suppress the nonradiative leap of trilinear excitons, and the doping of N and P elements facilitates the $n \rightarrow \pi^*$ leap, which promotes the inter-system crossover (ISC) and can effectively promote the radiative leap luminescence of trilinear excitons. Finally, the potential applications of

the prepared long afterglow luminescent material in the field of anti-counterfeiting were demonstrated experimentally, and the clear long afterglow fluorescence of celery, which can actively absorb the long afterglow luminescent material in a living state and transport it through vascular bundles, also verified its feasibility as a bioimaging probe.

Institutional Review Board Statement: Not applicable.

Informed Consent Statement: Not applicable.

Data Availability Statement: The data that support the findings of this study are available from the corresponding author upon reasonable request.

References

1. Cui, G.; Yang, X.; Zhang, Y.; Fan, Y.; Chen, P.; Cui, H.; Liu, Y.; Shi, X.; Shang, Q.; Tang, B. Round-the-Clock Photocatalytic Hydrogen Production with High Efficiency by a Long-Afterglow Material. *Angew. Chem. Int. Ed.* **2019**, *58*, 1340–1344. [CrossRef] [PubMed]
2. Miao, Q.; Xie, C.; Zhen, X.; Lyu, Y.; Duan, H.; Liu, X.; Jokerst, J.V.; Pu, K. Molecular afterglow imaging with bright, biodegradable polymer nanoparticles. *Nat. Biotechnol.* **2017**, *35*, 1102–1110. [CrossRef]
3. Yang, X.; Yan, D. Long-afterglow metal-organic frameworks: Reversible guest-induced phosphorescence tunability. *Chem. Sci.* **2016**, *7*, 4519–4526. [CrossRef] [PubMed]
4. Wang, L.; Shang, Z.; Shi, M.; Cao, P.; Yang, B.; Zou, J. Preparing and testing the reliability of long-afterglow $SrAl_2O_4$:Eu^{2+}, Dy^{3+} phosphor flexible films for temperature sensing. *RSC Adv.* **2020**, *10*, 11418–11425. [CrossRef] [PubMed]
5. Zhou, Y.; Lu, S.; Zhi, J.; Jiang, R.; Chen, J.; Zhong, H.; Shi, H.; Ma, X.; An, Z. Microscopic Afterglow Bioimaging by Ultralong Organic Phosphorescent Nanoparticles in Living Cells and Zebrafish. *Anal. Chem.* **2021**, *93*, 6516–6522. [CrossRef]
6. He, W.; Sun, X.; Cao, X. Construction and Multifunctional Applications of Visible-Light-Excited Multicolor Long Afterglow Carbon Dots/Boron Oxide Composites. *ACS Sustain. Chem. Eng.* **2021**, *9*, 4477–4486. [CrossRef]
7. Pan, M.; Liao, W.-M.; Yin, S.-Y.; Sun, S.-S.; Su, C.-Y. Single-Phase White-Light-Emitting and Photoluminescent Color Tuning Coordination Assemblies. *Chem. Rev.* **2018**, *118*, 8889–8935. [CrossRef] [PubMed]
8. Bilgic, A. Novel BODIPY-based fluorescent Lycopodium clavatum sporopollenin microcapsules for detection and removal of Cu(II) ions. *Colloids Surf. A Physicochem. Eng. Asp.* **2021**, *631*, 127658. [CrossRef]
9. Kursunlu, A.N.; Sahin, E.; Guler, E. Cu (II) Chemosensor Based on a Fluorogenic Bodipy-Salophen Combination: Sensitivity and Selectivity Studies. *J. Fluoresc.* **2016**, *26*, 1997–2004. [CrossRef]
10. Kursunlu, A.N. Synthesis and photophysical properties of modifiable single, dual, and triple-boron dipyrromethene (Bodipy) complexes. *Tetrahedron Lett.* **2015**, *56*, 1873–1877. [CrossRef]
11. Tao, Y.; Chen, R.; Li, H.; Yuan, J.; Wan, Y.; Jiang, H.; Chen, C.; Si, Y.; Zheng, C.; Yang, B.; et al. Resonance-Activated Spin-Flipping for Efficient Organic Ultralong Room-Temperature Phosphorescence. *Adv. Mater.* **2018**, *30*, e1803856. [CrossRef] [PubMed]
12. Hai, O.; Pei, M.; Yang, E.; Ren, Q.; Wu, X.; Zhu, J.; Zhao, Y.; Du, L. Exploration of long afterglow luminescence materials work as round-the-clock photocatalysts. *J. Alloys Compd.* **2021**, *866*, 158752. [CrossRef]
13. Hu, S.; Jiang, K.; Wang, Y.; Wang, S.; Li, Z.; Lin, H. Visible-Light-Excited Room Temperature Phosphorescent Carbon Dots. *Nanomaterials* **2020**, *10*, 464. [CrossRef] [PubMed]
14. Jiang, K.; Wang, Y.; Li, Z.; Lin, H. Afterglow of carbon dots: Mechanism, strategy and applications. *Mater. Chem. Front.* **2020**, *4*, 386–399. [CrossRef]
15. Gimenez, R.; Crespo, O.; Diosdado, B.; Elduque, A. Liquid crystalline copper(i) complexes with bright room temperature phosphorescence. *J. Mater. Chem. C* **2020**, *8*, 6552–6557. [CrossRef]
16. Jiang, K.; Wang, Y.; Gao, X.; Cai, C.; Lin, H. Facile, Quick, and Gram-Scale Synthesis of Ultralong-Lifetime Room-Temperature-Phosphorescent Carbon Dots by Microwave Irradiation. *Angew. Chem. Int. Ed.* **2018**, *57*, 6216–6220. [CrossRef]
17. Nidhankar, A.D.; Goudappagouda; Wakchaure, V.C.; Babu, S.S. Efficient metal-free organic room temperature phosphors. *Chem. Sci.* **2021**, *12*, 4216–4236. [CrossRef]
18. Xu, L.; Zhou, K.; Qiu, X.; Rao, B.; Pei, D.; Li, A.; An, Z.; He, G. Tunable ultralong organic phosphorescence modulated by main-group elements with different Lewis acidity and basicity. *J. Mater. Chem. C* **2020**, *8*, 14740–14747. [CrossRef]
19. Patir, K.; Gogoi, S.K. Long Afterglow Room-Temperature Phosphorescence from Nanopebbles: A Urea Pyrolysis Product. *Chem. Asian J.* **2019**, *14*, 2573–2578. [CrossRef]

20. Zhang, Y.; Sun, Q.; Yue, L.; Wang, Y.; Cui, S.; Zhang, H.; Xue, S.; Yang, W. Room Temperature Phosphorescent (RTP) Thermoplastic Elastomers with Dual and Variable RTP Emission, Photo-Patterning Memory Effect, and Dynamic Deformation RTP Response. *Adv. Sci.* **2022**, *9*, 2103402. [CrossRef]

21. Zhang, Y.-F.; Wang, Y.-C.; Yu, X.-S.; Zhao, Y.; Ren, X.-K.; Zhao, J.-F.; Wang, J.; Jiang, X.-Q.; Chang, W.-Y.; Zheng, J.-F.; et al. Isophthalate-Based Room Temperature Phosphorescence: From Small Molecule to Side-Chain Jacketed Liquid Crystalline Polymer. *Macromolecules* **2019**, *52*, 2495–2503. [CrossRef]

22. Gutierrez, M.; Martin, C.; Hofkens, J.; Tan, J.-C. Long-lived highly emissive MOFs as potential candidates for multiphotonic applications. *J. Mater. Chem. C* **2021**, *9*, 15463–15469. [CrossRef]

23. DeRosa, C.A.; Kolpaczynska, M.; Kerr, C.; Daly, M.L.; Morris, W.A.; Fraser, C.L. Oxygen-Sensing Difluoroboron Thienyl Phenyl beta-Diketonate Polylactides. *Chempluschem* **2017**, *82*, 399–406. [CrossRef]

24. Li, W.; Zhou, W.; Zhou, Z.; Zhang, H.; Zhang, X.; Zhuang, J.; Liu, Y.; Lei, B.; Hu, C. A Universal Strategy for Activating the Multicolor Room-Temperature Afterglow of Carbon Dots in a Boric Acid Matrix. *Angew. Chem. Int. Ed.* **2019**, *58*, 7278–7283. [CrossRef] [PubMed]

25. Wang, S.; Xu, M.; Huang, K.; Zhi, J.; Sun, C.; Wang, K.; Zhou, Q.; Gao, L.; Jia, Q.; Shi, H.; et al. Biocompatible metal-free organic phosphorescent nanoparticles for efficiently multidrug-resistant bacteria eradication. *Sci. China Mater.* **2020**, *63*, 316–324. [CrossRef]

26. Wang, Y.; Gao, H.; Yang, J.; Fang, M.; Ding, D.; Tang, B.Z.; Li, Z. High Performance of Simple Organic Phosphorescence Host-Guest Materials and their Application in Time-Resolved Bioimaging. *Adv. Mater.* **2021**, *33*, e2007811. [CrossRef] [PubMed]

27. Huang, Q.; Gao, H.; Yang, S.; Ding, D.; Lin, Z.; Ling, Q. Ultrastable and colorful afterglow from organic luminophores in amorphous nanocomposites: Advanced anti-counterfeiting and in vivo imaging application. *Nano Res.* **2020**, *13*, 1035–1043. [CrossRef]

28. Lu, C.; Su, Q.; Yang, X. Ultra-long room-temperature phosphorescent carbon dots: pH sensing and dual-channel detection of tetracyclines. *Nanoscale* **2019**, *11*, 16036–16042. [CrossRef]

29. Liang, Y.-C.; Gou, S.-S.; Liu, K.-K.; Wu, W.-J.; Guo, C.-Z.; Lu, S.-Y.; Zang, J.-H.; Wu, X.-Y.; Lou, Q.; Dong, L.; et al. Ultralong and efficient phosphorescence from silica confined carbon nanodots in aqueous solution. *Nano Today* **2020**, *34*, 100900. [CrossRef]

30. Tao, S.; Lu, S.; Geng, Y.; Zhu, S.; Redfern, S.A.T.; Song, Y.; Feng, T.; Xu, W.; Yang, B. Design of Metal-Free Polymer Carbon Dots: A New Class of Room-Temperature Phosphorescent Materials. *Angew. Chem. Int. Ed.* **2018**, *57*, 2393–2398. [CrossRef]

31. Wang, B.; Lu, S. The light of carbon dots: From mechanism to applications. *Matter* **2022**, *5*, 110–149. [CrossRef]

32. Zhang, B.; Liu, C.-Y.; Liu, Y. A Novel One-Step Approach to Synthesize Fluorescent Carbon Nanoparticles. *Eur. J. Inorg. Chem.* **2010**, *2010*, 4411–4414. [CrossRef]

33. Chai, Y.; Feng, Y.; Zhang, K.; Li, J. Preparation of Fluorescent Carbon Dots Composites and Their Potential Applications in Biomedicine and Drug Delivery—A Review. *Pharmaceutics* **2022**, *14*, 2482. [CrossRef]

34. Peng, H.; Travas-Sejdic, J. Simple Aqueous Solution Route to Luminescent Carbogenic Dots from Carbohydrates. *Chem. Mater.* **2009**, *21*, 5563–5565. [CrossRef]

35. de Medeiros, T.V.; Manioudakis, J.; Noun, F.; Macairan, J.-R.; Victoria, F.; Naccache, R. Microwave-assisted synthesis of carbon dots and their applications. *J. Mater. Chem. C* **2019**, *7*, 7175–7195. [CrossRef]

36. Liang, R.; Huo, L.; Yu, A.; Wang, J.; Jia, C.; Li, J. A micro-wave strategy for synthesizing room temperature phosphorescent materials. *Chin. Chem. Lett.* **2022**, *33*, 243–246. [CrossRef]

37. Jiang, K.; Gao, X.; Feng, X.; Wang, Y.; Li, Z.; Lin, H. Carbon Dots with Dual-Emissive, Robust, and Aggregation-Induced Room-Temperature Phosphorescence Characteristics. *Angew. Chem. Int. Ed.* **2020**, *59*, 1263–1269. [CrossRef] [PubMed]

38. Zhou, G.W.; Yang, J.C. In situ UHV-TEM investigation of the kinetics of initial stages of oxidation on the roughened Cu(110) surface. *Surf. Sci.* **2004**, *559*, 100–110. [CrossRef]

39. Patel, V.R.; Agrawal, Y.K. Nanosuspension: An approach to enhance solubility of drugs. *J. Adv. Pharm. Technol. Res.* **2011**, *2*, 81–87. [CrossRef]

40. Missana, T.; Adell, A. On the applicability of DLVO theory to the prediction of clay colloids stability. *J. Colloid Interface Sci.* **2000**, *230*, 150–156. [CrossRef]

41. Li, Y.; Gecevicius, M.; Qiu, J. Long persistent phosphors-from fundamentals to applications. *Chem. Soc. Rev.* **2016**, *45*, 2090–2136. [CrossRef]

42. Zhu, S.; Song, Y.; Zhao, X.; Shao, J.; Zhang, J.; Yang, B. The photoluminescence mechanism in carbon dots (graphene quantum dots, carbon nanodots, and polymer dots): Current state and future perspective. *Nano Res.* **2015**, *8*, 355–381. [CrossRef]

43. Zheng, C.; Tao, S.; Yang, B. Polymer-Structure-Induced Room-Temperature Phosphorescence of Carbon Dot Materials. *Small Struct.* **2023**, 2200327. [CrossRef]

44. Bilgic, A.; Cimen, A. A highly sensitive and selective ON-OFF fluorescent sensor based on functionalized magnetite nanoparticles for detection of Cr(VI) metal ions in the aqueous medium. *J. Mol. Liq.* **2020**, *312*, 113398. [CrossRef]

45. Sun, Y.; Zhang, X.; Zhuang, J.; Zhang, H.; Hu, C.; Zheng, M.; Lei, B.; Liu, Y. The room temperature afterglow mechanism in carbon dots: Current state and further guidance perspective. *Carbon* **2020**, *165*, 306–316. [CrossRef]

46. Wei, X.; Yang, J.; Hu, L.; Cao, Y.; Lai, J.; Cao, F.; Gu, J.; Cao, X. Recent advances in room temperature phosphorescent carbon dots: Preparation, mechanism, and applications. *J. Mater. Chem. C* **2021**, *9*, 4425–4443. [CrossRef]

47. Zhen, X.; Qu, R.; Chen, W.; Wu, W.; Jiang, X. The development of phosphorescent probes for in vitro and in vivo bioimaging. *Biomater. Sci.* **2021**, *9*, 285–300. [CrossRef]
48. Wolfbeis, O.S. An overview of nanoparticles commonly used in fluorescent bioimaging. *Chem. Soc. Rev.* **2015**, *44*, 4743–4768. [CrossRef] [PubMed]
49. Cai, P.; Zhang, X.; Wang, M.; Wu, Y.-L.; Chen, X. Combinatorial Nano-Bio Interfaces. *ACS Nano* **2018**, *12*, 5078–5084. [CrossRef]
50. Wang, W.; Sedykh, A.; Sun, H.; Zhao, L.; Russo, D.P.; Zhou, H.; Yan, B.; Zhu, H. Predicting Nano-Bio Interactions by Integrating Nanoparticle Libraries and Quantitative Nanostructure Activity Relationship Modeling. *ACS Nano* **2017**, *11*, 12641–12649. [CrossRef]